Tertiary lymphoid structures critical for prognosis in endometrial cancer patients - a TransPORTEC study

Nanda Horeweg (n.horeweg@lumc.nl)
Leiden University Medical Center https://orcid.org/0000-0002-8581-4753

Hagma Workel
University of Groningen

Dominik Loiero
University Hospital Zürich, University of Zürich https://orcid.org/0000-0002-0452-0068

David Church
Wellcome Centre for Human Genetics, University of Oxford and Oxford NIHR Comprehensive Biomedical Research Centre, Oxford University Hospitals NHS Foundation Trust

Lisa Vermij
Leiden University Medical Center

Alicia Léon-Castillo
Leiden University Medical Center

Ricki Krog
Leiden University Medical Center https://orcid.org/0000-0002-0201-7207

Stephanie de Boer
Leiden University Medical Center

Remi Nout
Erasmus MC Cancer Institute

Melanie Powel
Barts Health National Health Service Trust

Linda Mileshkin
Peter MacCallum Cancer Centre

Helen MacKay
University of Toronto

Alexandra Leary
Institute Gustave Roussy

Naveena Singh
Barts Health National Health Service Trust

Ina Jürgenliemk-Schulz
University Medical Center Utrecht

Carien Creutzberg
Leiden University https://orcid.org/0000-0002-7008-4321

Viktor Koelzer
University and University Hospital Zürich https://orcid.org/0000-0001-9206-4885
Hans Nijman
University Medical Center Groningen
Tjalling Bosse
Leiden University Medical Center
Marco Bruyn
University Medical Center Groningen

Article

Keywords: B-cells,endometrial cancer, cancer survival, tumors

DOI: https://doi.org/10.21203/rs.3.rs-677975/v1

Abstract

B-cells play a key role in cancer suppression, particularly when aggregated in tertiary lymphoid structures (TLS). Here, we investigated the role of B-cells and TLS in endometrial cancer (EC). Single cell RNA-sequencing of B-cells showed presence of activated/memory B-cells, cycling/germinal center B-cells and antibody-secreting cells. Differential gene expression analysis showed association of TLS with L1CAM overexpression. Immunohistochemistry and co-immunofluorescence showed L1CAM expression in mature TLS localized in the myometrial wall or at the tumor invasive border, independent of L1CAM expression the tumor. Using L1CAM as a marker, 378 of the 411 molecularly classified ECs from the PORTEC-3 biobank were evaluated. TLS were found in 19%, predominantly in mismatch-repair deficient and polymerase-epsilon mutant EC. Multivariable Cox regression analysis showed strong favorable prognostic impact of TLS, independent of clinicopathological and molecular factors. Our data suggests a pivotal role of TLS in outcome of EC patients, and establishes L1CAM as a simple biomarker.

Statement of significance Tertiary lymphoid structures have a pivotal role in the immune response against endometrial cancer. Presence of mature tertiary lymphoid structures can be easily assessed using L1CAM immunohistochemistry and has independent favorable predictive value for recurrence and endometrial cancer-specific survival.

Introduction

The molecular classification of endometrial cancer (EC) distinguishes four subtypes with validated prognostic impact: i) ultra-mutated EC with DNA-polymerase epsilon exonuclease domain mutations (*POLE*mut) with an excellent prognosis; ii) hypermutated EC with mismatch-repair deficiency (MMRd) with an intermediate prognosis; iii) copy-number-high EC with frequent *TP53* mutations (p53abn) with an unfavorable prognosis; and iv) copy-number-low EC without a specific molecular profile (NSMP) with an intermediate prognosis. We recently demonstrated that assessment of $CD8^+$ tumor infiltrating T-lymphocytes (TILs) improves prognostication beyond clinicopathological risk factors and molecular class.[1] In another study, we found that T-cell responses led to B-cell driven immune responses via the secretion of CLCX13, a key driver of B-cell recruitment.[2] Expression of CLCX13 was associated with the formation of B-cell aggregates in and around ECs in the presence of high endothelial venules (HEV), germinal B-cells centers and dendritic cells surrounded by a rim of T-cells.[2] This specific type of ectopic lymphoid formations are known as tertiary lymphoid structures (TLS).[3,4] At TLS, local and systemic B- and T-cell responses against cancer are initiated and maintained.[4,5] TLS presence is associated with a reduced risk of recurrence and improved response to immune checkpoint blockade (ICB) in several cancers.[5–11] A recent study assessed presence of TLS in EC by a 12-cytokine signature and identified most TLS in *POLE*mut and MMRd EC.[6] TLS were associated with a significantly better prognosis, but independence of this effect of clinicopathological features and molecular class was not assessed.[6] In this study, we aimed to better understand the role and prognostic relevance of B-cells and TLS in the immunity against EC.

Results

We first performed an in-depth analysis of B-cell responses in EC by single-cell mRNA sequencing (scRNA-seq) of 1501 B-cells obtained from 6 ECs (Fig. 1A). Unsupervised clustering identified three main clusters of B-cells characterized by: activation-induced genes including *HLA-DRA* and *IRF8* (cluster 1); Germinal Centre (GC)-like genes *HMGB2*, *BHLHE40* and *VIM* (cluster 2); and plasma cell genes *PRDM1*, *XBP1*, *IGHG1-4*, *IGHA1-2* and *CD38* (Cluster 3) (Fig. 1B). We assigned a probabilistic classification for each of the B-clusters to a lymph node spatial transcriptomics dataset, using a tonsil scRNA-seq dataset as control (Supplemental Fig. 1). Cluster 1 cells resembled activated/memory B-cells (ABC), cluster 2 cells cycling/GC B-cells (GC) and cluster 3 antibody-secreting cells (ASC) (Fig. 1C and Supplemental Fig. 1). Interestingly, ABCs did not only express classical activation markers such as *HLA-DRA*, but also *CD11c*, linked to chronic antigen stimulation and B-cell 'exhaustion' in auto-immune disease (Fig. 1D). We characterized the observed antibody responses in more detail and found 4 major ASC-clusters (Fig. 1E). The clusters were consistent with B-cell class switching and largely based on differential expression of heavy chain genes *IGHG1-4*, *IGHA1-2* and the mutually exclusive light chain genes *IGLC2-7* and *IGKC* (Fig. 1E). These observations are in line with a recent study in HPV-associated HNSCC[12], and suggest similarities between B-cell responses in viral- and neoantigen-driven immune responses.

The presence of ABC and GC B-cells raised the possibility that these could be a result of ongoing TLS formation. To confirm this, we quantified TLS using H&E-stained histological sections from The Cancer Genome Atlas (TCGA) uterine corpus endometrial cancer cohort (Fig. 2A). In line with previous observations[6,13], TLS were more common among the neoantigen-rich MMRd and *POLE*mut EC-subtypes (Fig. 2B). Differential gene expression analysis revealed a significantly higher expression of genes associated with $CD8^+$-T-cell infiltration (*CD8A*) and effector function (*LAG3*, *CCL5*, *NKG7*, *GZMH*) in ECs with TLS (Fig. 2C and Supplemental Table 1). Surprisingly, we also noted significantly greater expression of *L1CAM* in ECs with TLS (Fig. 2C). L1CAM overexpression of cancer cells is associated with increased metastatic potential and worse prognosis.[14] We followed up on this observation by performing L1CAM-immunohistochemistry (IHC) on EC samples (Fig. 2D). We observed strong L1CAM staining in the GC-like structures of the TLS, which co-localized with follicular dendritic cell (FDC) marker CD21 (Fig. 2E). This was independent of L1CAM overexpression by the tumor. Analysis of sequential tissue sections confirmed presence and typical distribution of TLS hallmark immune cell subsets in aggregates expressing L1CAM (Supplemental Figure S2).

To explore whether expression of L1CAM could be used as a marker for the presence of mature TLS, we used the L1CAM-stained whole tissue slides of the PORTEC-3 trial.[15] In 378 of the 411 molecularly classified ECs, L1CAM-stained slides of sufficient quality were available for TLS assessment (Figure S3, Table S2). Using this method, TLS were observed at the tumor invasive border and in the myometrium in 71 of the 378 EC tissues (18.8%), ranging from 1 to 20 TLS per slide (median 2). As in the TCGA cohort, presence of TLS was correlated with the neoantigen-rich *POLE*mut and MMRd molecular subtypes (Fig. 3A, Table S3). Moreover, in EC's with multiple classifying features, such as MMRd EC with secondary p53-

abnormality, TLS were more common (Fisher Exact p = 0.009) and more abundant (Mann-Whitney p = 0.013, Table S3). While $CD8^+$ and $CD20^+$ densities were also significantly higher among *POLE*mut and MMRd ECs, only a subset had TLS (Fig. 3A, Table S4-6). Both the intraepithelial and the intrastromal densities of CD8 + T-cells showed a significant and independent correlation with TLS presence, while only the intrastromal density of CD20 + B-cells was weakly associated with TLS presence and lost significance after correction for clinicopathological features and molecular class (Table S7).

Next, we assessed the prognostic impact of $CD8^+$ and $CD20^+$-cell densities and TLS among PORTEC-3 participants. For $CD8^+$, both the intraepithelial and the intrastromal densities were strongly associated with a lower risk of recurrence (per doubling of density: HR 0.85, 95%CI 0.78–0.93, p = 0.00049 and HR 0.87, 95%CI 0.80–0.95, p = 0.0046 respectively), while only intrastromal $CD20^+$ density was significantly associated with a lower recurrence risk (HR 0.92, 95%CI 0.85-1.00, p = 0.048; Table S8). Both the number and presence (none vs. ≥1) of TLS were strongly associated with a reduced risk of recurrence (HR 0.62, 95%CI 0.42–0.92, p = 0.017 and HR 0.25, 95%CI 0.10–0.62, p = 0.0028). Based on the effect size and model fit (Table S8) and the significant correlations between variables (Table S9) we decided to proceed with the dichotomous TLS variable.

Presence of TLS was a significant favorable prognostic factor for both time to endometrial cancer recurrence (Fig. 3B) and endometrial cancer-related death (Fig. 3C). Five-year risk of recurrence was 7.2% (95%CI 0.9–13.1%) with TLS compared to 32.6% (95%CI 27.1–37.7%) without TLS. To determine whether prognostic impact of TLS was independent, we built a multivariable Cox proportional hazards model including the molecular classifier and all relevant clinicopathological features of high-risk EC (according to Léon-Castillo et al.[16], Fig. 4A). TLS was a significant and independent favorable predictor of recurrence (HR 0.32, 95%CI 0.14–0.73, p = 0.0073) and endometrial cancer-specific survival (HR 0.15, 95%CI 0.04–0.61, p = 0.0085; Fig. 4A, Table S10). Addition of TLS to the prognostic model published by Léon-Castillo et al. significantly improved model fit (Fig. 4B-C). Explorative subgroup analysis by molecular group (Fig. 3D-E) showed a significant favorable prognostic impact of TLS in MMRd EC (p = 0.003).

To verify whether TLS, rather than CD8 + or CD20 + densities, are the best addition to clinicopathological factors and molecular class in prediction model, we performed a sensitivity analysis. We compared TLS with the strongest immune cell density markers for $CD8^+$ (intraepithelial) and $CD20^+$ (intrastromal). Using cases with all 3 immuno-biomarkers available (n = 252), 3 multivariable Cox proportional hazards models were built in resemblance of the final molecular-immune model (Fig. 4A). These models showed (Table S10) that intrastromal $CD20^+$ density had no independent prognostic impact after correction for clinicopathological factors and molecular class (HR 0.98, 95%CI 0.91–1.07, p = 0.69). Intraepithelial $CD8^+$ density had independent prognostic impact (HR 0.89, 95%CI 0.80–0.99, p = 0.029) but model fit was less good (concordance-index 0.736, se 0.027) than with TLS (0.745, se 0.026); likelihood ratio-test for nested models $p = 2.20x10^{-16}$).

Discussion

In this study, we leveraged scRNA-seq of B-cells in EC to establish the presence of activated/memory B-cells, cycling/germinal center B-cells and antibody-secreting B-cells. The antibody-secreting B-cells had undergone class-switching and expressed markers of activation and exhaustion, suggesting TLS formation and an ongoing B-cell response against EC. Differential gene expression analysis showed an association of TLS with $CD8^+$ T-cell infiltration and L1CAM overexpression. IHC analysis of L1CAM-stained whole tumor slides showed ectopic lymphoid structures at the tumor invasive border and the myometrium that expressed L1CAM independent of any L1CAM expression by the tumor itself. The L1CAM-expressing lymphoid structures appeared to be mature TLS with a germinal center, based on co-immunofluorescence and IHC for hallmark immune cell subsets. Using L1CAM expression at lymphoid structures as a marker, we assessed tumor material of 378 high-risk EC patients included in the PORTEC-3 trial and found TLS in 19% of cases.[15] Subsequent analyses confirmed the favorable prognostic impact of TLS in an independent randomized trial with high quality clinical outcome data (PORTEC-3), which was previously only demonstrated in the TCGA dataset[6] and a small retrospective study[17]. We are the first to demonstrate that presence of TLS remains a strong favorable prognostic factor after correction for all important clinicopathological and molecular risk factors.

The mechanisms behind the favorable prognostic impact of TLS has only partially been explained in endometrial and other cancers. It is known that TLS orchestrate a specific and coordinated immune reaction that results in a high density of mature dendritic cells, tumor-infiltrating lymphocytes (TILs) and effector-memory CD8 + T-cells.[5,18] T-cell:B-cell interactions in the TLS contribute to T-cell activation and maturation of B-cells to antibody producing plasma cells.[3,5,19] In addition, immunologic memory is generated that can mediate systemic immune surveillance against metastasis.[18]

Knowledge of the specific conditions that promote TLS formation is important to advance towards identification of targetable mechanisms. Specifically, the observation that TLS are more frequently present in *POLE*mut and MMRd ECs by us and others[6] supports the hypothesis that TLS may form in reaction to immunogenic tumor neoantigens, which are more likely to be present in cancers with high mutational burden.[6] The observation that TLS were relatively common among ECs with multiple classifying features may support this hypothesis because recent work in transgenic *POLE*mut mice suggested that co-occurring MMRd or *TP53* mutations help *POLE*mut cancer cells to cope with a high mutational burden and may drive a higher neoantigen load.[20,21] However, the fact that we also observed TLS in p53abn and NSMP EC suggests that conditions favorable for TLS formation can also occur, though infrequently, in cancers with a relatively low mutational burden.

The observed co-localization of L1CAM and CD21 may also shed light on the formation of TLS. CD21 demarcates FDCs, which are thought to originate from perivascular precursor cells, that undergo activation and maturation in response to lymphotoxin (LT) beta receptor signaling. As perivascular cells use L1CAM to migrate across the endothelial basal lamina, it is tempting to speculate that L1CAM-positive perivascular cells may represent FDC precursors in human tumors. A sequence of events could be envisioned where tumor-reactive T-cells release CXCL13[2,20], attracting CXCR5 + LT + immune cells to

the perivascular space initiating L1CAM-positive perivascular cell activation and maturation to FDCs. Subsequent production of CXCL13 and inflammatory cytokines, chemokines and upregulation of cell adhesion molecules[22–24] including ICAM-2/3, VCAM-1 and MAdCAM-1 would mediate recruitment and adhesion of additional lymphocytes via high endothelial venules.[24] Together with recruitment of other immune cells such as dendritic cells and innate lymphoid cells, stroma maturation and stabilization into lymphoid stroma is promoted and TLS may form.[22,23]

Bringing insights into the tumor microenvironment back to clinical practice is challenging, as the analysis methods used in studies are often not available in routine diagnostics. For example, gene signatures identified from transcriptomic analysis, such as the 12-cytokine signature for TLS[6,19], have been validated for TLS identification but are resource-demanding and difficult to implement. At the same time, use of H&E-stained slides has been shown to be poorly reproducible between pathologists.[25] Combined immunohistochemical stains of TLS-hallmark immune cell subsets can be performed, but are inconvenient to quantify.[9] In contrast, TLS detection by a single immunohistochemical staining for L1CAM is simple to implement in clinical trials and routine diagnostics.

To conclude, we here demonstrate that presence of mature tertiary lymphoid structures, as assessed using L1CAM immunohistochemistry, improves prediction accuracy of recurrence and death beyond clinicopathological risk factors and molecular class in high-risk endometrial cancer patients.

Methods

Patient material

The scRNA-seq analysis were performed using endometrial cancer digests obtained from surgical waste material of patients treated at University Medical Center Groningen, the Netherlands in accordance with local medical ethical guidelines and after written informed consent. All material was processed and stored anonymously. According to Dutch law, no approval from our institutional review board was needed.

Clinical data and tumor material from high-risk endometrial cancer patients participating in the randomized PORTEC-3 trial have been used (ISRCTN14387080, NCT00411138). The design and results of the PORTEC-3 trial have been published.[15] Briefly, 660 patients were included (2006–2013) with: FIGO-2009 stage IA endometrioid endometrial cancer grade 3 with lymph-vascular space invasion; or stage IB endometrioid endometrial cancer grade 3; or endometrioid endometrial cancer stage II, IIIA, IIIB (parametrial invasion) or IIIC; or stage I to III endometrial cancer with serous or clear cell histology. Written informed consent has been obtained from all patients. The study protocol was approved by the Ethics Committees of all participating groups and is available online at: http://msbi.nl/portec3

Immunohistochemistry

L1CAM-stained whole tumor slides were available in the PORTEC-3 biobank; procedures of immunohistochemical staining have been published.[14] For the assessment of $CD8^+$ and $CD20^+$ densities, TMAs were produced as previously described.[2] Immunohistochemistry for $CD8^+$ and $CD20^+$ was carried out using a modification of a previously reported protocol.[1,2] Antigen retrieval was performed in a preheated 10 mmol/L citrate buffer (pH = 6) and endogenous peroxidase activity was blocked by 0.45% hydrogen-peroxide. Slides were blocked in PBS containing 1% human serum and 1% BSA. Slides were incubated overnight with mouse anti-human CD8 (3 mg/L, clone C8/144B, GA62361–2, DAKO, Agilent Technologies) or anti-CD20 (0.63 mg/L; clone L26, catalog number M0755, Dako) at 4°C. Subsequently, slides were incubated with a ready-to-use peroxidase-labelled polymer for 30 minutes (Envision+/HRP anti-mouse, K4001, Dako). Specific signal was visualized with 3,3'diaminobenzidin (DAB) and slides were counterstained with hematoxylin. Appropriate washing steps with PBS were performed in-between incubation steps. Sections were embedded in Eukitt mounting medium (Sigma Aldrich), and slides were scanned on a Hamamatsu digital slide scanner (Hamamatsu Photonics).

Quantification of L1CAM-positive TLS

TLS were quantified by an expert gynecopathologist (TB) blinded for clinicopathological and molecular data. A TLS was counted when an organized lymphoid aggregate with any L1CAM positivity in the center was observed in the myometrial wall or at the tumor invasive border. Lymphoid aggregates without any L1CAM positivity were not counted.

Machine learning-based quantification and localization of $CD8^+$ and $CD20^+$ cells

Procedures have been published previously.[1] Briefly, two pathologists (DL, VHK) performed digital slide review and quality control. Spots with staining artefacts, folds or < 1,000 cells/spot were excluded. Digital image analysis was performed using HALO digital image analysis software v3.0.311.355 (Indica Labs, Corrales, NM, USA). TMA slides were segmented into individual spots and linked to clinical information. By annotating tissue regions, a deep neural network algorithm was trained to localize and quantify tumor epithelial tissue and tumor-associated stroma regions. Classification accuracy was confirmed after generation of graphical overlays for each tissue area. Cell and staining quantification were carried out with following specifications: Nuclei (hematoxylin, RGB 20, 24, 65),CD8 (DAB, RGB 122, 93, 65), CD20 (DAB, RGB-102, 73, 60). Unstained epithelium and stromal fibroblasts served as internal negative controls. Marker positive cells were then allocated to the tumor or stroma compartment and infiltration density (cells/mm^2), was recorded. Final scores for each case were calculated as the mean of the infiltration densities across all cores. Average densities were $\log_2$ transformed and negative values for $\log_2$ transformed densities were imputed with 0 before analysis to approximate a normal distribution. Concordance between pathologist estimation and artificial intelligence-based quantification has been demonstrated.[1]

Single-cell RNA sequencing

Tumors were cut into ca. $1cm^3$, enzymatically digested in RPMI medium (Gibco, Paisley, UK) with 1 mg/µL collagenase type IV (Gibco Life Technologies, Grand Island, USA) and 12,6 µg/mL recombinant human

DNase (Pulmozyme, Roche, Woerden, the Netherlands) for 30 minutes at 37°C or overnight at room temperature. Digests were filtered using 70µm cell strainers (Falcon) and enriched for peripheral blood mononuclear cells (PBMCs) using Ficoll-Paque PLUS (GE Healthcare Life Sciences, Marlborough, MA, USA). Cells were stored in liquid nitrogen until cell sorting. For cell sorting, tumor digests were thawed and washed with PBS and incubated with Zombie Aqua (1:100, Biolegend, San Diego, USA) for 15 minutes at room temperature. Samples were washed and stained with anti-CD27 APC-efluor 780 (clone O323; 47-0279-42; eBioscience) and either CD19-PE (clone HIB19; 12-0199-41; eBioscience), CD19-BV421 (clone HIB19; 562440; BD Biosciences), CD19-APC (clone HIB19; 17-0199-41; eBioscience) or CD19-PE-cy7 (clone HIB19; 25-0199-41; eBioscience) for 45 minutes at 4°C. Cells were washed and filtered using a 35µm strainer (Falcon). Patient samples were pooled to minimize differences due to plate effects and sorted on a Beckman Coulter MoFlo Astrios. Each well contained 2µl lysis buffer (0.2% Triton X-100 (Sigma-Aldrich) and 2U RNase inhibitor (Takara)) with 1µl 10µM oligo-dT primer and 1µl 10mM dNTP mix (Thermo Scientific). After sorting, the plate was spun down and incubated at 72°C for 3 minutes. We used a modified SMARTseq2 protocol using custom-made primers. SmartScribe reverse transcriptase (Westburg-Clontech) and a template switching oligo (BC-TSO) were used to generate cDNA. Next, an exonuclease step was performed using 1:400 dilution of Exonuclease I. A PCR preamplification step was done with KAPA HiFi HotStart Ready Mix (Roche Diagnostics, 23 cycles in experiment 1 and 25 cycles in experiment 2) and a custom-made PCR primer. The cDNA samples were purified using Ampure XP beads (Beckman Coulter) in a ratio of 0.8:1 (Ampure bead:cDNA). Samples were analyzed on a 2100-Bioanalyzer using a PerkinElmer LabChip GX high-sensitivity DNA chip (Agilent) and on a Qubit™ 4 Fluorometer (ThermoFisher Scientific) according to manufacturer's instructions. 500pg of each sample was tagmented and N7xx and S5xx index adapters were used for barcoding according to the Illumina Nextera XT DNA sample preparation kit (Illumina). Thereafter, samples were purified with Ampure XP beads (ratio 0.6:1 Ampure:cDNA) and analyzed on a 2100-Bioanalyzer. Samples were equimolar pooled (4nM) and samples were sequenced on an Illumina Nextseq500 2500 using 75bp paired end reads. The obtained mRNA sequencing data was demultiplexed into individual FASTQ files followed by alignment to the human reference genome hg38 using STAR (version 2.5.2).

Processing and annotation of single-cell and spatial RNA-seq

Single-cell sequencing data was analyzed in R (Seurat (V4) package). Data were quality controlled, normalized, scaled and analyzed for annotation by running PCA, nearest neighbor graph (FindNeighbors) and unbiased clustering (FindClusters) with default settings. Uniform Manifold Approximation and Projection (UMAP) was used to visualize B cell clusters. Gene expression markers for different clusters of B cells were identified using FindAllMarkers from Seurat with default settings, including Wilcoxon test and Bonferroni p-value correction, and plotted by heatmap (DoHeatmap). Antibody-secreting cells were then separated for a more detailed annotation by recomputing the PCA (RunPCA), nearest neighbor graph (FindNeighbors) and unbiased clustering (FindClusters). UMAP and FeaturePlots were used to visualize the IGHG, IGHA and IGLC and IGKC clusters. For spatial analysis, we used human lymph node Visium data available through the 10x Genomics website (https://support.10xgenomics.com/spatial-gene-expression/datasets/). A previously published (King et al. Sci Immunol. 2021) tonsil scRNA-seq dataset

(E-MTAB-9005) was used to assign cellular identity to spatial location using the ‘anchor’-based integration workflow from Seurat. Hereto, data was scaled and normalized using SCTransform with default parameters, followed by the probabilistic identification (FindTransferAnchors) and transfer (TransferData) of annotations from the tonsil scRNA-seq to the lymph node Visium data. The same unmodified workflow was followed for the integration of EC scRNA-seq data with the lymph node Visium data.

Differential gene expression analysis of UCEC TCGA data

MRNA-seq and clinical data from uterine corpus endometrial carcinoma (UCEC) were downloaded from firebrowse.org. TLS were quantified using H&E images of the UCEC TCGA cohort downloaded from https://portal.gdc.cancer.gov. Differentially expressed genes were assessed between TLS-positive and TLS-negative MMRd and POLE-EDM cases by DESeq2 (version 2_1.30.0). Genes with a Benjamini–Hochberg FDR < 0.01 and log2 fold change > 1 were selected as significantly different.

Statistical analysis

Biomarker analyses were performed in accordance with the REMARK guidelines and are listed in Supplementary Table S11. Primary endpoint was time to endometrial cancer recurrence, defined as time from randomization to recurrence, with censoring at last follow-up in case of no recurrence. Secondary endpoint was endometrial cancer-specific survival, defined as time from randomization to endometrial cancer death, with censoring at last follow-up in alive patients.

Continuous variables were analyzed by either parametric or nonparametric methods depending on their distribution. Categorical variables were analyzed by nonparametric methods. Correlations were assessed using the Spearman correlation coefficient. Hierarchical clustering was used (Ward minimum variance method with Euclidean distances) to group CD8 and CD20 densities stratified by molecular class. Median follow-up was calculated by the reverse Kaplan–Meier method. Time-to-event analyses were performed by the Kaplan-Meier method, log-rank tests and multivariable Cox proportional hazards models. Clinicopathological and molecular variables for inclusion in multivariable models were prespecified based on the model published by Léon-Castillo et al.[16] Model validation was performed by analysis of discrimination and indices of optimism determined by means of model fitting to 1000 bootstrap resamples. Proportionality of hazards was confirmed by inspection of scaled Schoenfeld residuals. Relative importance of variables within the multivariable models is based on the proportion of the χ^2 statistic. Statistical significance was accepted at $p < 0.05$ (two-sided). Statistical analyses were performed in SPSS version 25 and R Version 3.6.3. using i.a. the following packages: ComplexHeatmap, rms, Survival, ggPlot2, Survminer, Hmisc and tidyverse.

Declarations

Author contributions

Design: NH, DC, VK, HN, TB, MdB

Data and material: LV, ALC, SdB, MP, LM, HM, AL, NS, IJS, CC, HN, MdB

Experiments: HW, DL, DC, RK, VK, TB, MdB

Statistical analysis: NH, DL, DC, VK, MdB

Manuscript writing: NH, MdB

Critical manuscript review: HW, DL, DC, SdB, RN, CC, VK, HN, TB

Conflicts of interests statement

Dr. Horeweg reports outside of the submitted work to have received research grants from the Dutch Cancer Society.

Dr. Church reports to be part of the advisory board for MSD.

Prof. Koelzer reports having served as an invited speaker on behalf of Indica Labs.

Dr. de Bruyn reports, outside the submitted work, having received grants from the Dutch Cancer Society (KWF), grants from the European Research Council (ERC), grants from Health Holland, grants from DCPrime, non-financial support from BioNTech, non-financial support from Surflay, non-financial support from MSD, grants and non-financial support from Vicinivax. In addition, dr. de Bruyn has grants and non-financial support from Aduro Biotech, in part relating to a patent for Antibodies targeting CD103 (de Bruyn et al. No. 62/704,258).

Funding

This work was supported by the Dutch Cancer Society: project grant RUG 2015-7235 and project grant 8232-21648. This work was supported by* The Oxford NIHR Comprehensive Biomedical Research Centre (BRC) and WHG core funding from the Wellcome Trust (203141/Z/16/Z). Dr. Church is funded by a Cancer Research UK Advanced Clinician Scientist Fellowship (C26642/A27963).

Prof. Koelzer reports grants from Promedica Foundation (F-87701-41-01) during the conduct of the study.

* The views expressed are those of the authors and not necessarily those of the NHS, the NIHR, the Department of Health

Data availability

The code and parts of the data that support the findings of this study are available on request from the corresponding author (NH). The PORTEC data are not publicly available due to patient privacy and consent restrictions.

References

1. Horeweg, N.*, et al.* Prognostic Integrated Image-Based Immune and Molecular Profiling in Early-Stage Endometrial Cancer. *Cancer Immunol Res* **8**, 1508-1519 (2020).

2. Workel, H.H.*, et al.* A Transcriptionally Distinct CXCL13(+)CD103(+)CD8(+) T-cell Population Is Associated with B-cell Recruitment and Neoantigen Load in Human Cancer. *Cancer Immunol Res* **7**, 784-796 (2019).

3. Dieu-Nosjean, M.C., Goc, J., Giraldo, N.A., Sautes-Fridman, C. & Fridman, W.H. Tertiary lymphoid structures in cancer and beyond. *Trends Immunol* **35**, 571-580 (2014).

4. Dieu-Nosjean, M.C.*, et al.* Tertiary lymphoid structures, drivers of the anti-tumor responses in human cancers. *Immunol Rev* **271**, 260-275 (2016).

5. Goc, J., Fridman, W.H., Hammond, S.A., Sautes-Fridman, C. & Dieu-Nosjean, M.C. Tertiary lymphoid structures in human lung cancers, a new driver of antitumor immune responses. *Oncoimmunology* **3**, e28976 (2014).

6. Lin, Z.*, et al.* Pan-cancer analysis of genomic properties and clinical outcome associated with tumor tertiary lymphoid structure. *Sci Rep* **10**, 21530 (2020).

7. Di Caro, G.*, et al.* Occurrence of tertiary lymphoid tissue is associated with T-cell infiltration and predicts better prognosis in early-stage colorectal cancers. *Clin Cancer Res* **20**, 2147-2158 (2014).

8. Kroeger, D.R., Milne, K. & Nelson, B.H. Tumor-Infiltrating Plasma Cells Are Associated with Tertiary Lymphoid Structures, Cytolytic T-Cell Responses, and Superior Prognosis in Ovarian Cancer. *Clin Cancer Res* **22**, 3005-3015 (2016).

9. Cabrita, R.*, et al.* Tertiary lymphoid structures improve immunotherapy and survival in melanoma. *Nature* **577**, 561-565 (2020).

10. Petitprez, F.*, et al.* B cells are associated with survival and immunotherapy response in sarcoma. *Nature* **577**, 556-560 (2020).

11. Helmink, B.A.*, et al.* B cells and tertiary lymphoid structures promote immunotherapy response. *Nature* **577**, 549-555 (2020).

12. Wieland, A.*, et al.* Defining HPV-specific B cell responses in patients with head and neck cancer. *Nature* (2020).

13. Talhouk, A.*, et al.* Molecular Subtype Not Immune Response Drives Outcomes in Endometrial Carcinoma. *Clin Cancer Res* **25**, 2537-2548 (2019).

14. Van Gool, I.C.*, et al.* Prognostic significance of L1CAM expression and its association with mutant p53 expression in high-risk endometrial cancer. *Mod Pathol* **29**, 174-181 (2016).

15. de Boer, S.M.*, et al.* Adjuvant chemoradiotherapy versus radiotherapy alone for women with high-risk endometrial cancer (PORTEC-3): final results of an international, open-label, multicentre, randomised, phase 3 trial. *Lancet Oncol* **19**, 295-309 (2018).

16. Leon-Castillo, A.*, et al.* Molecular Classification of the PORTEC-3 Trial for High-Risk Endometrial Cancer: Impact on Prognosis and Benefit From Adjuvant Therapy. *J Clin Oncol* **38**, 3388-3397 (2020).

17. Shimizu, Y.*, et al.* The Prognostic Significance of Peritumoral Lymphocytes' Band-like Structure in Type II Endometrial Cancer. *Anticancer Res* **41**, 249-258 (2021).

18. Gunderson, A.*, et al.* Germinal center reactions in tertiary lymphoid structures associate with neoantigen burden, humoral immunity and long-term survivorship in pancreatic cancer. *Oncoimmunology* **10**, 1900635 (2021).

19. Germain, C.*, et al.* Presence of B cells in tertiary lymphoid structures is associated with a protective immunity in patients with lung cancer. *Am J Respir Crit Care Med* **189**, 832-844 (2014).

20. Thommen, D.S.*, et al.* A transcriptionally and functionally distinct PD-1(+) CD8(+) T cell pool with predictive potential in non-small-cell lung cancer treated with PD-1 blockade. *Nat Med* **24**, 994-1004 (2018).

21. Li, H.D.*, et al.* A PoleP286R mouse model of endometrial cancer recapitulates high mutational burden and immunotherapy response. *JCI Insight* **5**(2020).

22. Barone, F.*, et al.* Stromal Fibroblasts in Tertiary Lymphoid Structures: A Novel Target in Chronic Inflammation. *Front Immunol* **7**, 477 (2016).

23. Nayar, S.*, et al.* Immunofibroblasts are pivotal drivers of tertiary lymphoid structure formation and local pathology. *Proc Natl Acad Sci U S A* **116**, 13490-13497 (2019).

24. de Chaisemartin, L.*, et al.* Characterization of chemokines and adhesion molecules associated with T cell presence in tertiary lymphoid structures in human lung cancer. *Cancer Res* **71**, 6391-6399 (2011).

25. Buisseret, L.*, et al.* Reliability of tumor-infiltrating lymphocyte and tertiary lymphoid structure assessment in human breast cancer. *Mod Pathol* **30**, 1204-1212 (2017).

Figures

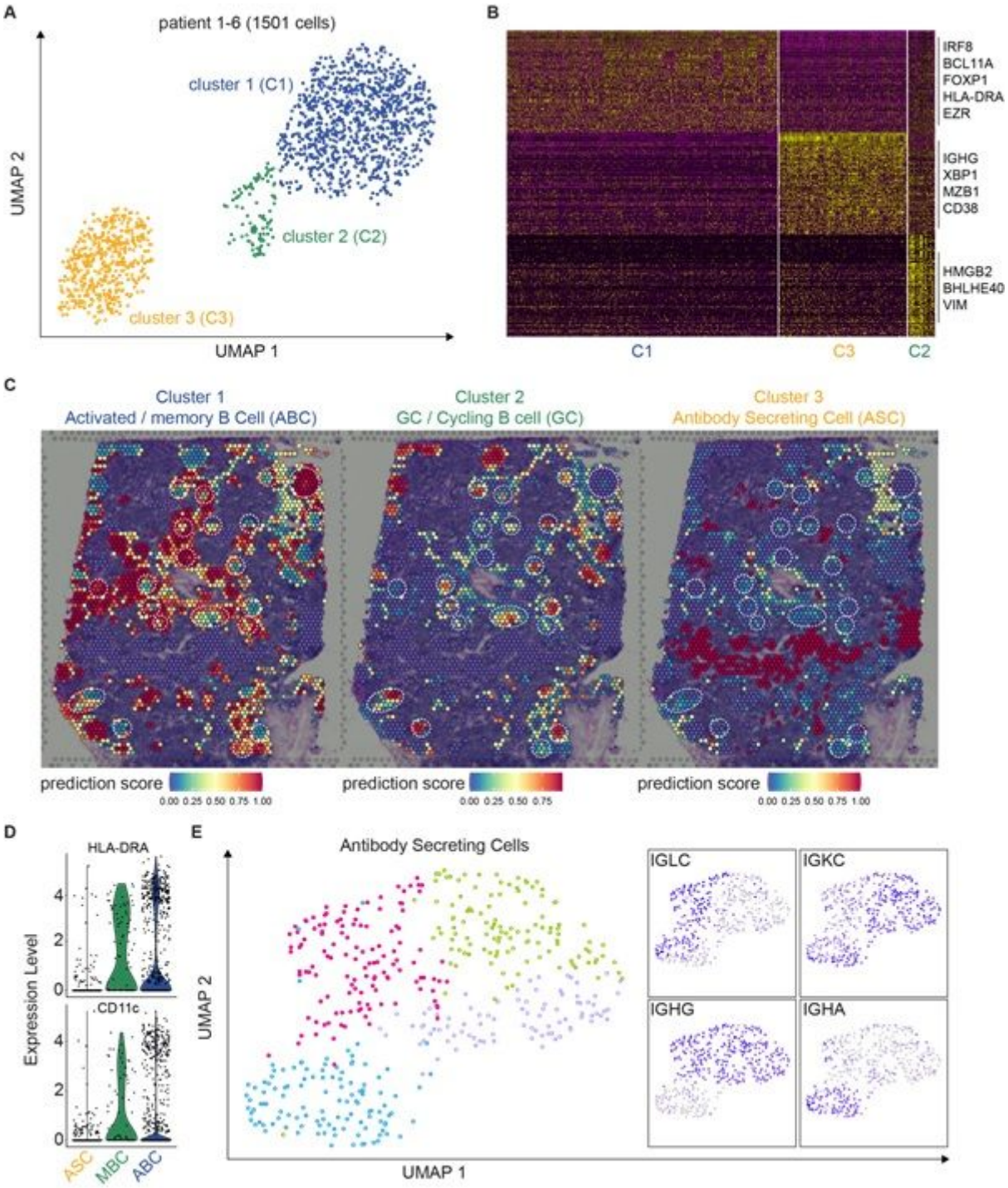

Figure 1

Single cell RNA sequencing of tumor-infiltrating B-cells. Panel A: UMAP projection of endometrial cancer B-cell scRNA-seq data (1501 cells; 6 donors) annotated by cluster. Panel B: Single-cell gene expression heatmap of differentially expressed genes per cluster ordered by log2 fold change within each cluster. Panel C: probabilistic classification for Cluster 1, Cluster 2 and Cluster 3 cells in spatial transcriptomic data of a human lymph node. Dashed circles represent germinal centers manually assigned on H&E. Panel D: Single-cell gene expression of HLA-DRA and CD11c in ABC, MBC and ASC cells. Panel E: UMAP

projection of ASCs with Feature Plots depicting IGHG, IGHA, IGLC and IGKC expression in single cells. Definition of abbreviations: ABC = activated B-cell, MBC = memory B-cell, ASC = Antibody-secreting cells.

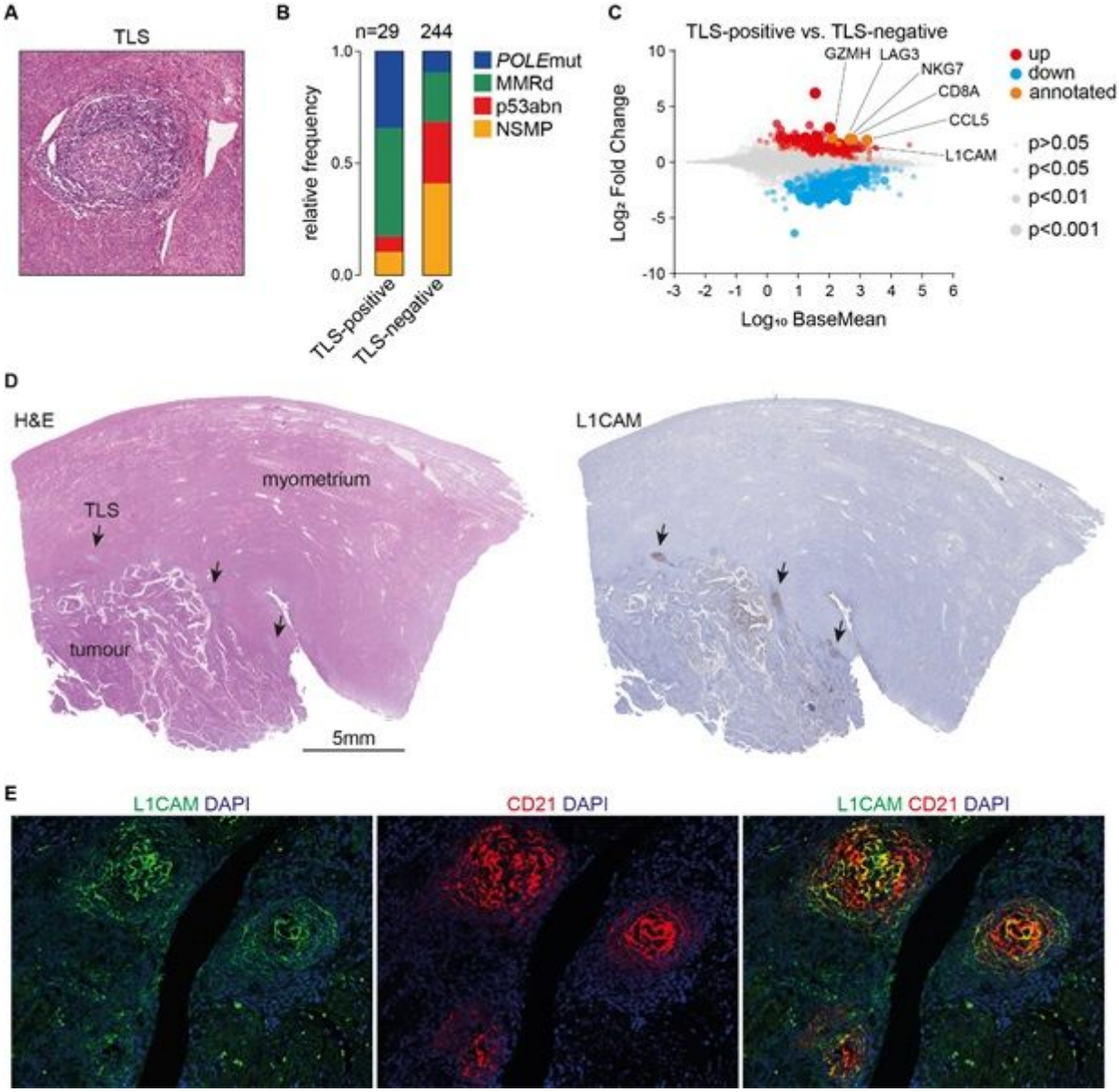

Figure 2

L1CAM expression in mature germinal centers of tertiary lymphoid structures. Panel A: Representative H&E image of a TLS in EC. Panel B: Frequency of molecular subgroups within TLS-positive and TLS-negative UCEC TCGA cases. Panel C: Differential gene expression of TLS-positive versus TLS-negative TCGA UCEC cases. Panel D: Representative L1CAM-positive TLS case. Arrows indicate TLS. Panel E: Co-immunofluorescent analysis of L1CAM-positive TLS with L1CAM and CD21. Definition of abbreviations: POLEmut = pathogenic polymerase epsilon mutation; MMRd = mismatch repair deficient; p53abn = p53 abnormal; NSMP = no specific molecular profile; TLS = tertiary lymphoid structure; L1CAM = ligant-1 cell adhesion molecule.

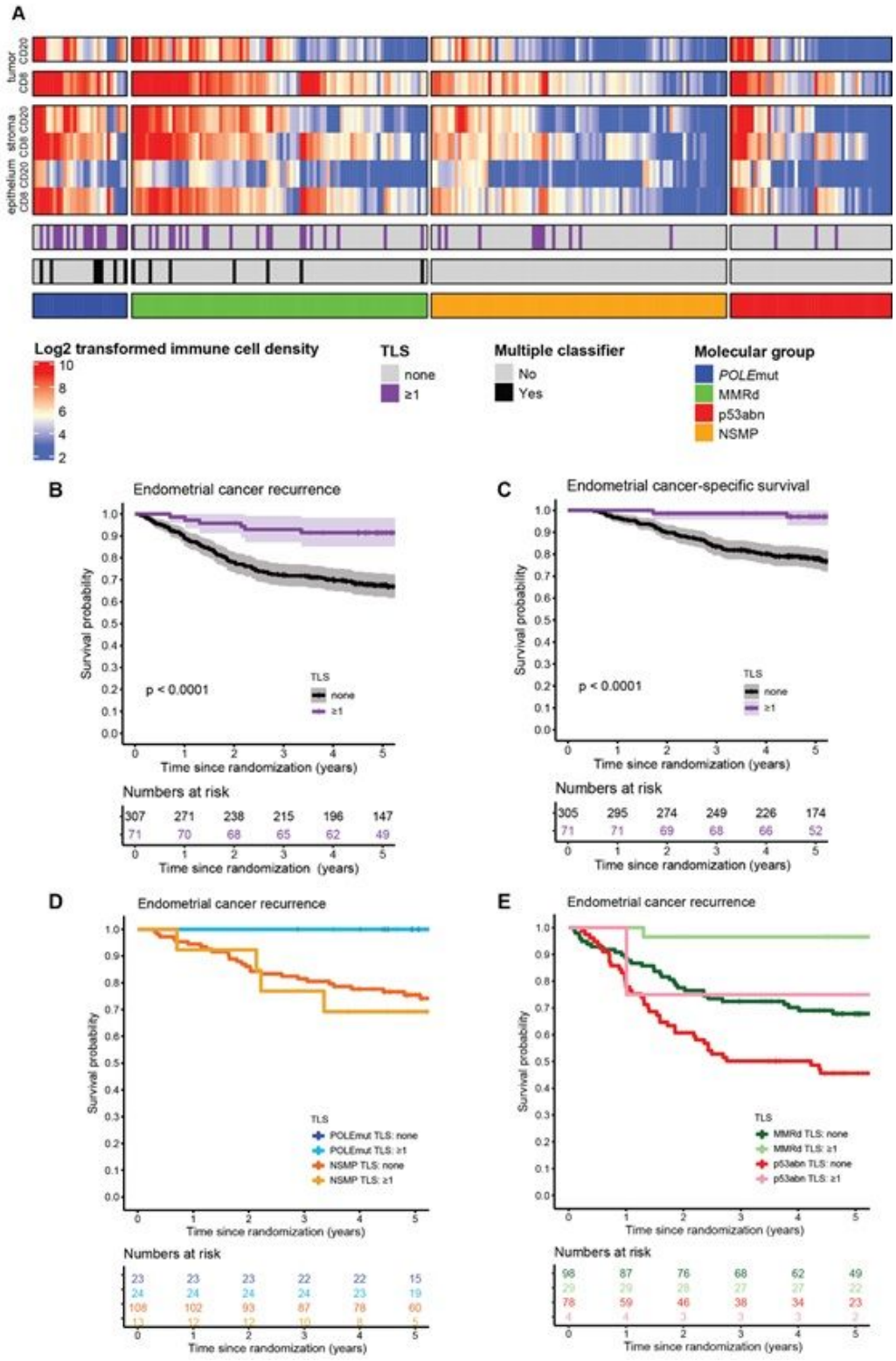

Figure 3

Relation between molecular group, TLS and CD8 densities and prognosis in high risk endometrial cancer. Panel A: heat map of included PORTEC 3 patients (N = 378) with available data on molecular classification, TLS, CD8+ and CD20+ densities (N = 252). Each patient is represented by a row in the graph. Clustering of CD8+ and CD20+ densities stratified by molecular group was done by hierarchical clustering using Ward's minimum variance method. Panel B-D: Recurrence-free survival probability

calculated according to Kaplan-Meier's methodology for B) all included PORTEC 3 patients (N = 378); C: included patients with POLEmut (N = 47) and MMRd endometrial cancer (N = 127); D) included patients with p53abn (N = 83) and NSMP endometrial cancer (N = 121). Definition of abbreviations: TLS = tertiary lymphoid structure; POLEmut = pathogenic polymerase epsilon mutation; MMRd = mismatch repair deficient; p53abn = p53 abnormal; NSMP = no specific molecular profile.

A

Recurrence	Pathologic model			Molecular model			Molecular-immune model		
n=378, 111 events	HR	95% CI	p value	HR	95% CI	p value	HR	95% CI	p value
Age	1.05	1.02-1.07	0.00032	1.03	1.00-1.05	0.045	1.03	1.00-1.05	0.034
Adjuvant treatment									
RT	reference								
CTRT	0.76	0.52-1.10	0.15	0.70	0.48-1.03	0.069	0.72	0.50-1.063	0.093
Histograde									
EEC grade 1-2	reference			reference			reference		
EEC grade 3	1.24	0.76-2.02	0.40	1.23	0.71-2.14	0.45	1.37	0.79-2.37	0.27
non-EEC	1.42	0.89-2.27	0.14	0.94	0.53-1.70	0.85	1.02	0.57-1.82	0.96
Stage (I-II vs. III)	1.93	1.28-2.91	0.0016	1.90	1.27-2.85	0.0020	1.98	1.31-2.97	0.0011
LVSI	1.25	0.82-1.96	0.30	1.29	0.83-2.00	0.25	1.24	0.80-1.94	0.33
Molecular group									
NSMP				reference			reference		
POLEmut				no events			no events		
MMRd				0.89	0.53-1.48	0.64	0.99	0.59-1.64	0.96
p53abn				2.63	1.46-4.73	0.0012	2.42	1.35-4.32	0.0029
TLS							0.32	0.14-0.73	0.0073

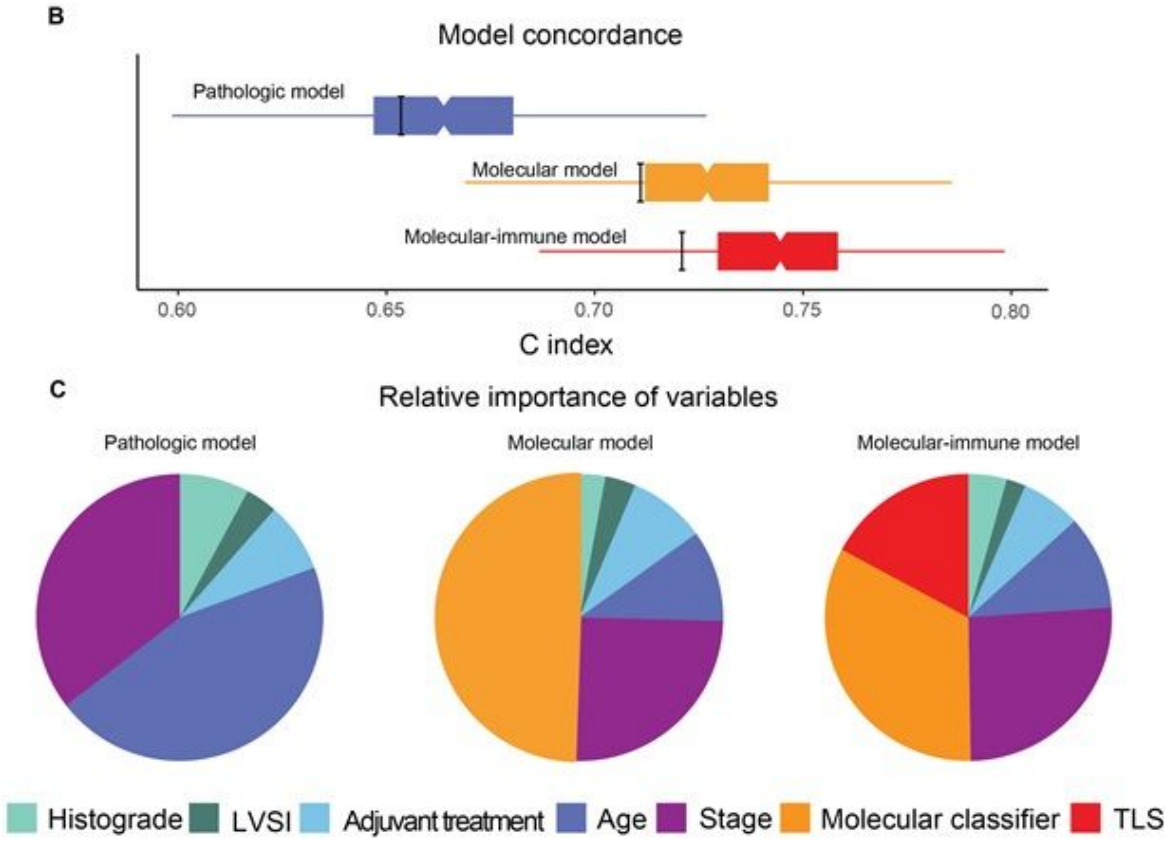

Figure 4

Prognostic factors in high risk endometrial cancer. Panel A: Three Cox proportional hazards models to showing impact of respectively clinicopathological factors, clinicopathological + molecular factors, and clinicopathological + molecular factors + presence of tertiary lymphoid structures on time to recurrence. Covariates were pre-specified according to Léon-Castillo et al. (J Clin Oncol, 2020). The addition of the molecular classifier to the pathologic model was associated with an improvement in model fit evidenced by: (i) reduction in Akaike's information criterion (AIC) 1244.968 vs. 1202.158, (ii) increase in model concordance (C index 0.655 vs. 0.714, and (iii) likelihood ratio test for comparison of nested models p = 1.43 x 10-10. Likewise, the addition of TLS presence improved model fit: (i) AIC 1202.158 vs. 1194.242, (ii) C index 0.714 vs. 0.729, (iii) likelihood ratio test for nested models p = 0.0016. Panel B: Boxplots showing concordance (C index) of the pathologic model, molecular model and the molecular-immune model. Box and whisker (Tukey) plots use results of 1,000 bootstrap resamples from study population; lower and upper limits of box indicate 25th and 75th percentiles; and whiskers extend to 1.5x interquartile range below and above these values, respectively. The thick black bars indicate the C index from original population. Panel C: Pie charts showing relative importance of variables within these three multivariable models based on the proportion of the $\chi 2$ statistic. Definition of abbreviations: HR = hazard ratio; CI = confidence interval; RT = external beam radiotherapy; CTRT = chemoradiotherapy; EEC = endometrioid endometrial cancer; LVSI = lymphovascular space invasion; NSMP = no specific molecular profile; POLEmut = pathogenic polymerase epsilon mutation; MMRd = mismatch repair deficient; p53abn = p53 abnormal; TLS = tertiary lymphoid structure

Supplementary Files

This is a list of supplementary files associated with this preprint. Click to download.

- Supplementaldata.pdf
- TableS1.GenesdifferentiallyexpressedbetweenTLSpositiveandTLSnegativeUCECTCGAcases.xlsx